

Measuring Chip Segmentation by High-Speed Microvideography and Comparison to Finite-Element Modeling Simulations

R. Ivester^{1*}, E. Whitenton¹, J. Heigel¹, T. Marusich², C. Arthur²

¹National Institute of Standards and Technology^a, Gaithersburg, Maryland, 20899-8223 USA

²Third Wave Systems, Minneapolis, Minnesota, 55439 USA

*ivester@nist.gov

Abstract

This paper presents comparisons between finite element modeling and experimental measurement of chip segmentation in American Iron and Steel Institute 1045 steel. Direct measurements of chip segmentation through post-process microscopic analysis or indirect observations of secondary phenomena such as acoustic emissions provide limited insight into chip formation. This paper presents measurements based on high-speed microvideography of orthogonal disk cutting, which provides direct spatial and temporal observation of dynamic chip formation mechanisms. The results show that segment spacing grows nearly linearly with surface speed. Finite element modeling (FEM) simulations provide a physics-based method for exploring the effectiveness of proposed mechanisms for explaining changes in cutting behavior with processing conditions. The FEM simulations yielded higher average segmentation frequencies with lower variability than the experiments, but they did agree within the range of experimental variation.

1 INTRODUCTION

Extensive research publications report on the post-process analysis of segmented (or sawtooth) chip formation by microscopic examination of cross-sectioned machined chips [1,2,3]. Much of this work focused on the segmented chip formation process in hardened steels [4,5,6,7], but other publications presented work on titanium [8,9], aluminum [10], and other materials of engineering or academic interest.

Other measurement techniques applied to the characterization of dynamic segmented chip formation at industrially relevant cutting speeds at or above 500 mm/s include various quick-stop techniques [11], acoustic techniques [12], and piezoelectric techniques [13]. Additionally, other researchers have explored the use of a scanning electron microscope to characterize chip formation at low cutting speeds [14].

Physical mechanisms for explaining the occurrence of segmentation during chip formation and other high strain-rate phenomena include localized thermoplastic instability [4,5,13] and crack propagation from the free surface of the chip [15,16,17]. Experimental evidence presented herein appears to support thermoplastic instability as the most likely explanation for segmented chip formation under these conditions, but alternative mechanisms could lead to segmentation for different workpiece and tool materials or different tool geometries.

This paper presents a novel experimental technique for observing chip formation processes at high magnification (approximately 1 mm field-of-view) and high frame rate (60 000 frames/s). The magnification and frame rate combination used in this study provides adequate spatial-temporal resolution for direct observation of material deformation patterns while metal cutting at surface speeds up to 10 m/s.

Finite-element modeling of the chip formation process using Third Wave Systems' Advant-Edge commercial software^a provides a physics-based simulation of chip segmentation based on thermoplastic instability [18]. A comparison of the experimental results presented in this paper to the simulation results provides insight into the strengths and limitations of both the experiments and the simulations.

2 EXPERIMENTAL SETUP

A modified grinding platform provides the test bed for orthogonal turning tests. The grinding platform allows a workpiece to be bolted to the spindle and lowered onto a stationary cutting tool. Workpieces are 2.74 mm thick, 127 mm

^a Commercial equipment and materials are identified in order to adequately specify certain procedures. In no case does such identification imply recommendation or endorsement by the National Institute of Standards and Technology, nor does it imply that the materials or equipment are necessarily the best available for the purpose. This paper is an official contribution of the National Institute of Standards and Technology and is not subject to copyright in the United States.

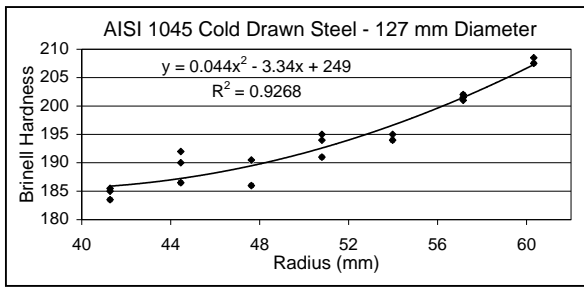


Figure 1: Typical radial hardness profile.

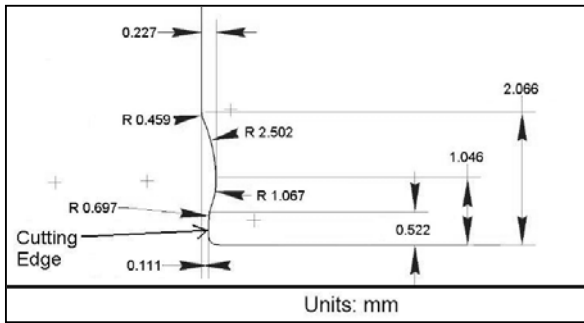


Figure 2: Insert chip breaker cross section.

diameter discs cut from American Iron and Steel Institute (AISI) 1045 cold-drawn steel rods. Grinding the disc surfaces ensured parallelism. Hardness of the cold-drawn workpiece material increased with radius (Figure 1).

Commercially available Seco-Carboly^a TNMG220408-MR4 CP25 triangular inserts, held in a -7° rake angle MTCNN443 tool holder and attached to the face of a 3-axis Kistler^a dynamometer, provide the orthogonal cutting edge for the experiments. The insert chip breaker geometry limits the chip contact length for each test to 0.552 mm (Figure 2).

A digital oscilloscope records the dynamometer signals at a sampling rate of 2 MHz before down sampling to 15 kHz for analysis. The stationary tool and cameras allow chip formation during the entire test duration to be filmed without inducing camera vibration. A high-speed camera and a digital camcorder simultaneously record the cutting tests from different perspectives. The high-speed camera (shutter speed of 60 000 frames/s, integration time of 1/500 000 s) provides an orthogonal view of the metal cutting process. The digital camcorder (shutter speed of 60 frames/s, integration time of 1/60 s) uses a bore scope to view the rake face of the tool. The high-speed camera provides a microscopic view of material flow from the workpiece into the chip, while the digital camcorder shows a top view of the chip formation. Synchronizing the dynamometer, high-speed camera, and camcorder signals at 2

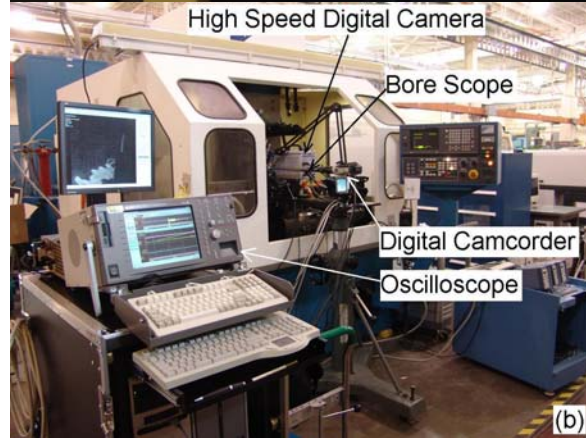
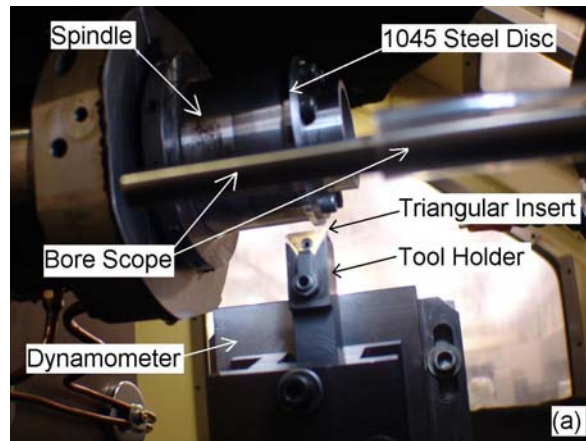


Figure 3: Experimental setup; perspective from inside the machine (a), and shop floor (b).

2 MHz provides confidence that measurements represent nearly identical instances in time. Figure 3 shows the experimental setup.

3 EXPERIMENTAL MEASUREMENTS

3.1 Force measurement interpretation

Figure 4 illustrates the typical cutting, thrust, and axial forces obtained from the dynamometer during one cutting test. Near-zero average axial forces ensure an orthogonal setup. Additionally, the frequency content of the three force signals provides useful information.

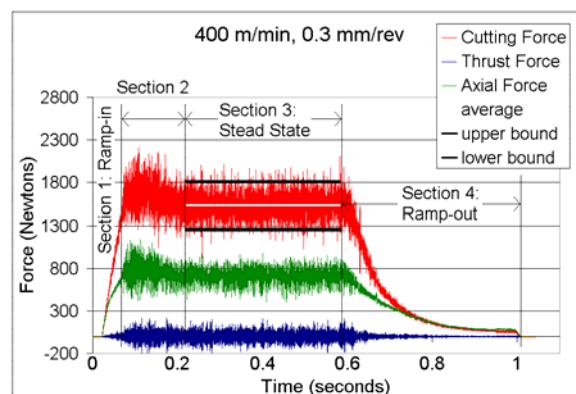


Figure 4: Sample force measurement.

The cutting and thrust forces can be broken into four sections: 1) ramp-in, 2) dynamic response, 3) steady state, and 4) ramp-out. The ramp-in section takes approximately 1 revolution, indicating an approximately linear feed increase. Section 2 contains a brief and moderate force increase before steady state. This peak in both the cutting and thrust forces can be attributed to the combined dynamic response of the machine and controller.

Section 3 represents steady state cutting, where the average cutting and thrust forces remain stable. The white line shows the average steady state cutting force and the black lines indicate variability of the individual measurements using a coverage factor of 2 [19].

The workpiece disengages from the cutting tool during section 4. Note the nonlinearity of the disengagement, unlike the engagement in section 1. Although sections 1 and 4 include variable feed rate cutting, this paper focuses on the steady state cutting in section 3 of Figure 4.

3.2 Segmentation determination

Chip segmentation is determined manually by analyzing 1000 consecutive frames of video from the start of steady state cutting as determined by the force signal analysis. Figure 5 shows the progression of three (3) frames of video during the formation of a new segment to illustrate that the camera integration time is adequate to minimize motion-induced blur and that the frame rate is adequate to effectively capture the deformation pattern by tracking the movement of surface features between frames.

Figure 5 represents the typical chip segment formation determined by repeated frame-by-frame viewings of the cutting videos. These videos show that incoming workpiece material adheres to and builds up on the rake face. The build-up of adhered material causes the material behind it to rotate as it flows around the stopped material; some depositing onto the stopped material, increasing its size, and some pushing the previous segment along the rake face of the tool. Eventually adhesion stress, shearing stresses, and flow stresses become unstable, leading to a new segment shearing itself from the incoming material. Visually, a new segment occurs when a crevice forms between the workpiece surface and the expelled chip (Figure 5C), and when the adhered material begins to slide up the rake face. In the electronic version of this document, Figure 6 presents an embedded movie of this process.

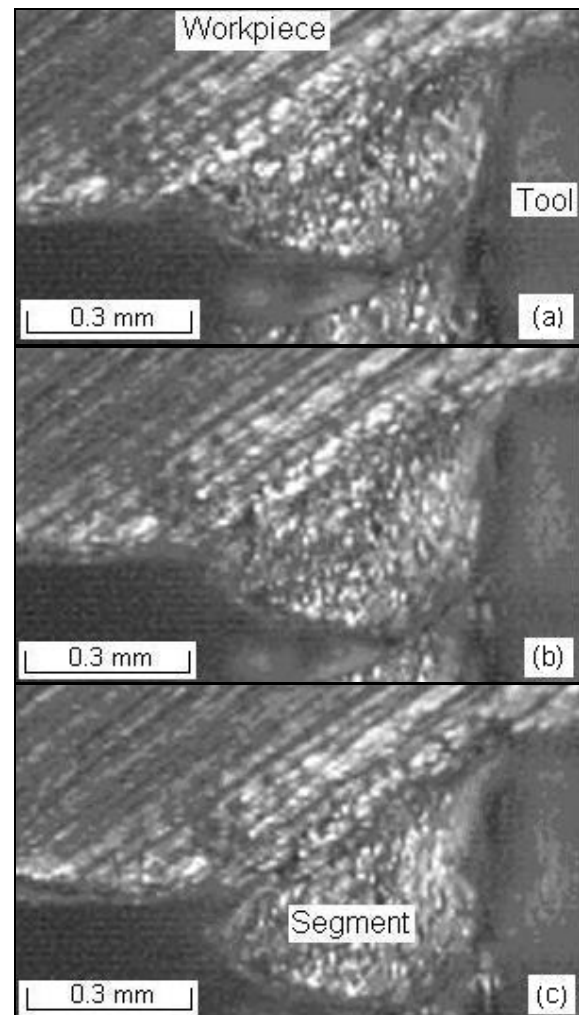


Figure 5: Segment formation progression; velocity = 400 m/min, feed = 0.3 mm/rev.

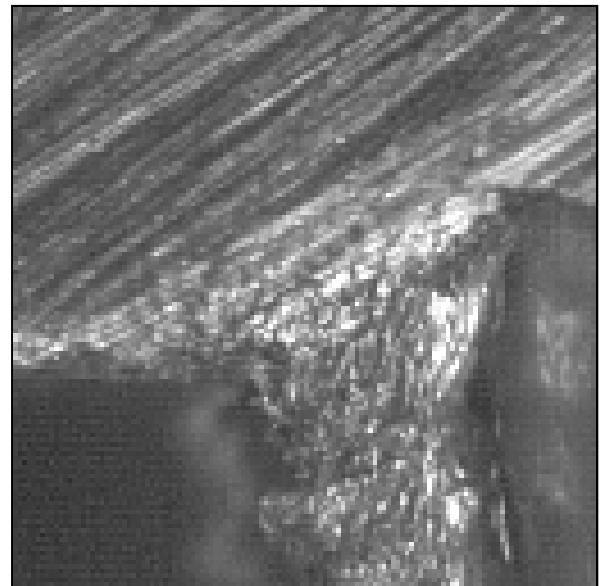


Figure 6: Segment formation embedded video; velocity = 400 m/min, feed = 0.3 mm/rev.

The high-speed video evidence shown in this research supports the concept of a dynamic stick / slip interface between the tool and chip. In this case, the chip adheres or sticks to the tool, starting at the edge of the tool and progressing along the rake face as the segment rotates or rolls on to the rake face. This sticking region spreads from the edge of the tool along the rake face as a new segment forms. The slipping region consists of the remainder of the contact length, or the contact area between the previously formed segments and the rake face. Due to the segmented chip formation, the stick / slip zones on the rake face change dynamically as a function of the thermoplastic instability in the stresses required to form a new segment. Formation of a new segment occurs when the shear stresses between the workpiece, the strain-hardened workpiece material built-up on the rake face, and the adjacent segment exceed the combination of adhesion and kinetic friction. Figure 7 illustrates the observed segmentation formation process.

In this study of a negative rake tool cutting steel, the secondary shear zone expected along the chip-tool interface is not visible. The build-up of adhered material and the associated rotation about this zone is a highly dynamic deformation pattern where extremely large plastic strains occur along the rake face and between adjacent segments, leading to the deformed chip structure commonly observed through post-process microscopic analysis.

Figure 8 displays the number of segments encountered as a function of the number of frames that have been counted. The linearity of datasets in this plot shows a lack of dynamic effects on segmentation frequency. To additionally justify the number of frames used, 1000 frames (0.017 s) prevents significant effects from workpiece preheating because the workpiece has not made a complete revolution during the steady state section, and is typically only a few revolutions into the test.

4 FINITE ELEMENT SIMULATIONS

4.1 Simulation conditions

Finite Element Modeling (FEM) simulations are performed using the workpiece material model for AISI 1045 steel at 200 BHN, and a custom coated carbide tool to match the insert geometry from Figure 2. Both deformation simulations and force plots show effects of segmentation. Figure 9 shows the degree of segmentation found in a simulation run at 400 m/min and

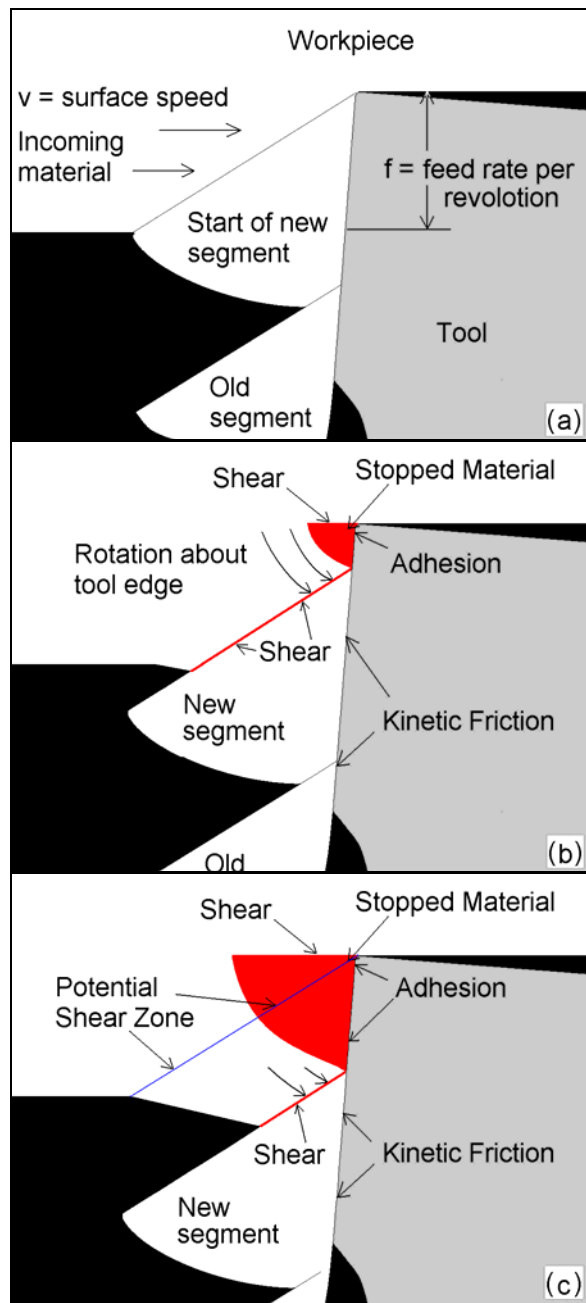


Figure 7: Segmentation formation illustration.

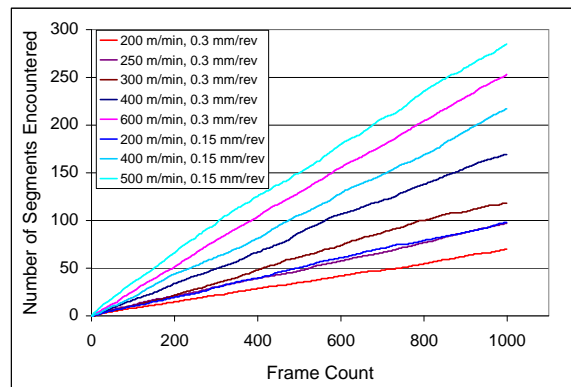


Figure 8: Video frame progression of segmentation.

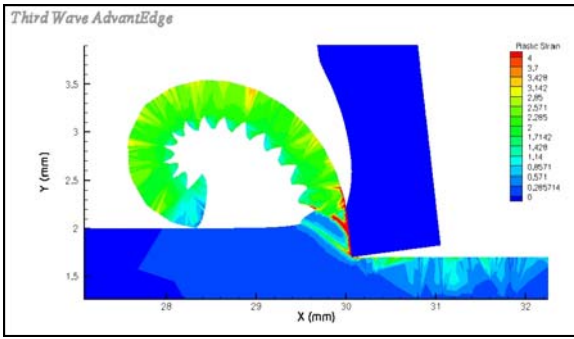


Figure 9: Segmentation of chip in simulation.

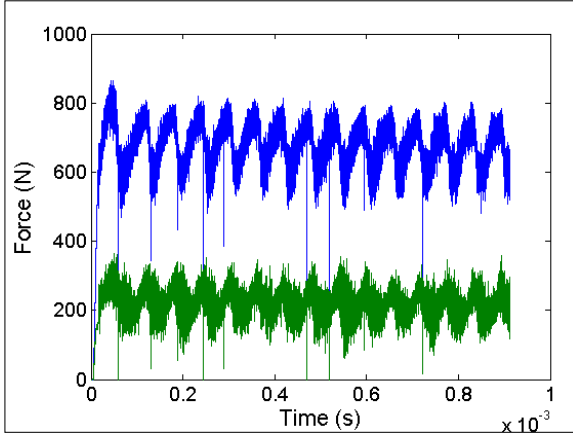


Figure 10: Simulated cutting (above) and thrust (below) forces for a depth of cut of 1 mm.

0.3 mm/rev feed. The unit rev (revolution) is used in place of 2π radians because it relates more directly to the machining process and manufacturing community. The corresponding force plot in Figure 10 shows effects of the segmentation in the force oscillations. The high points of the force oscillations together with the cutting speed lead to the simulation average segmentation frequency and average workpiece length per segmentation, a parameter to be defined later.

4.2 Segmentation mechanism

In the FEM simulations, highly localized increases in temperature cause thermal softening, which leads to chip segmentation through a propagation of localized shear-induced temperature increase and material softening. The workpiece material modeling does not include a material damage model. These results support the idea that thermoplastic instability causes chip segmentation for these cutting materials and conditions.

5 RESULTS

5.1 Steady state force analysis

Table 1 shows measured and simulated cutting and thrust forces. Simulation cutting forces exceed the measured cutting forces by about

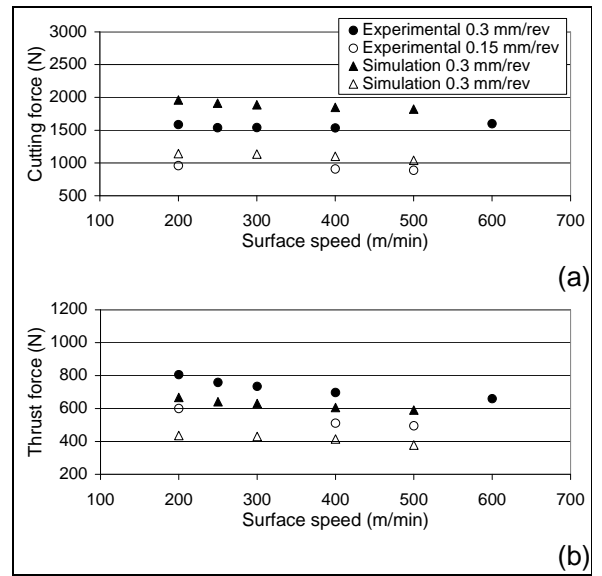


Figure 11: Force comparison to surface speed.

20 %, while the measured thrust forces exceed the simulation thrust forces by about 20 %. Figure 11 shows the relationships between the cutting and thrust forces and surface speed for both the simulations and experiments. The cutting forces remain relatively constant for the surface speeds ranging from 200 m/min to 600 m/min for both feeds. The simulated and measured thrust forces decrease with increasing speed for 0.15 mm and 0.30 mm feeds.

5.2 Segmentation analysis

Table 2 and Table 3 show the segmentation analysis for the simulations and the experiments. This paper presents two methods for analyzing the segmentation data, the time period between segments and workpiece length between segments.

Segmentation period

Equation 1 calculates the segmentation period (P_i) using the number of frames between two segments (N_i) and frame rate in frames/s (R).

$$P_i = \frac{N_i}{R} \quad (1)$$

Figure 12a shows the decreasing non-linear relationship between mean segmentation period and surface speed. Both experimental and simulation result trends agree, though the simulation data consistently shows a lesser mean period. Figure 12b and Figure 12c illustrate the relationship between mean segmentation period and cutting and thrust forces, respectively. Similar trends between measured and simulated data are once again shown in the relationship with thrust force; however, the trends do not agree for the cutting force in Fig-

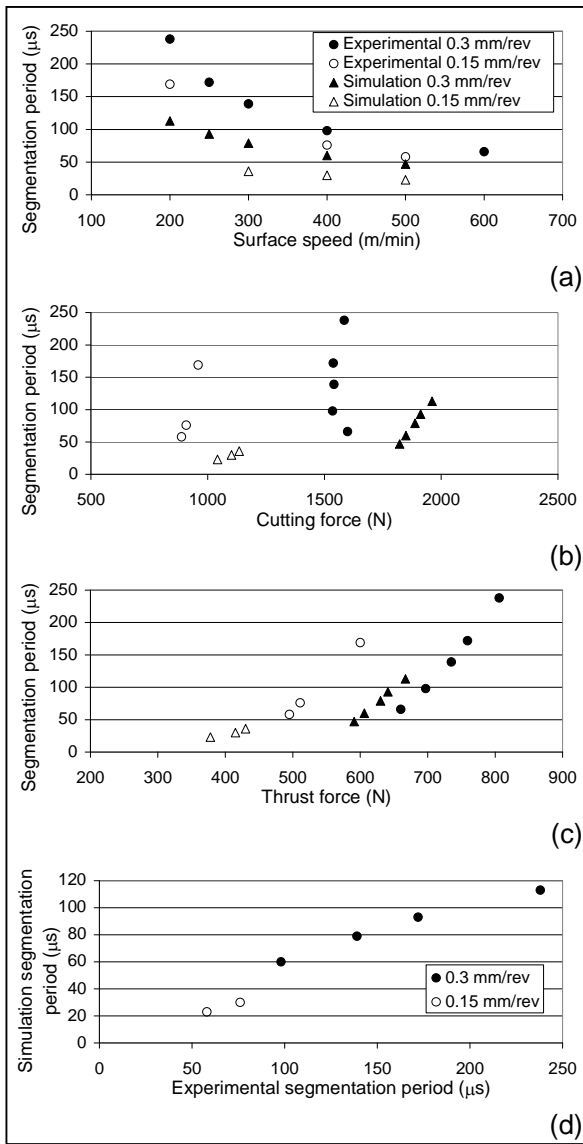


Figure 12: Example cutting and thrust forces from simulation.

Figure 12b. Here a positive slope linear relationship could be applied to the simulated data which is not present in the measured data. Finally, Figure 12d shows a direct comparison between the simulation and experimental results. The linear relationship between the two sources of data reaffirms that the simulations provide a trend that correlates to experimental results.

Workpiece length per segment

The length of workpiece between segments increases linearly with cutting speed. Equation 2 determines the length of workpiece material per segment (L_i) using surface speed (v). L is the mean workpiece length per segment.

$$L_i = \frac{N_i 1000v}{60R} \quad (2)$$

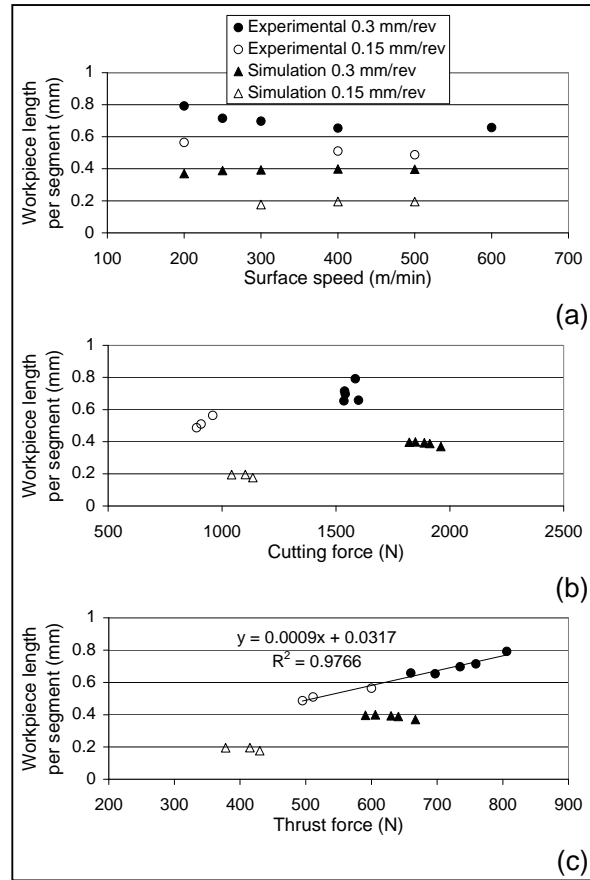


Figure 13: Example cutting and thrust forces from simulation.

Figure 13 shows that L decreases moderately with increasing surface speed. Figure 13a shows a difference in experimental and simulation trends for a feed of 0.3 mm/rev where the experimental L decreases and becomes constant while the simulation L increases then remains constant. Figure 13b does not show an obvious relation between L and cutting force. Figure 13c shows a nearly linear relationship between L and thrust force for the experimental data, independent of feed rate.

6 DISCUSSION

The experimental results demonstrate significant new insight into the process of chip segmentation. During the formation of the chip segment, the material adheres to the rake face, and the chip segment rotates around the cutting edge towards the rake face as the next segment forms. The friction model in the FEM simulations does not fully capture the dynamics of the oscillation in the relative velocity between the chip and the tool along the rake face, but does show chip segmentation. The average period of chip segmentation in the simulations is longer than in the experiments, but is within

the relatively broad range of segmentation periods observed in the experiments.

7 ACKNOWLEDGEMENTS

The authors acknowledge the support of Alkan Donmez and Hans Soons of the National Institute of Standards and Technology.

8 REFERENCES

- [1] Ernst, H., 1938, Physics of Metal Cutting, Machining of Metals, American Society for Metals, 1/1:1-34.
- [2] Field, M., Merchant, M.E., 1949, Mechanics of Formation of the Discontinuous Chip in Metal Cutting, Transactions of the ASME, 71/1:421-430.
- [3] Tonshoff, H.K., Arendt, C., Ben Amor, R., 2000, Cutting of Hardened Steel, Annals of the CIRP, 49/2:547-566.
- [4] Komanduri, R. Schroeder, T., Hazra, J., von Turkovich, B.F., Flom, D.G., 1982, On the Catastrophic Shear Instability in High-Speed Machining of an AISI 4340 Steel, Journal of Engineering for Industry, Transactions of ASME, 104/1:121-131.
- [5] Davies, M.A., Chou, Y., Evans, C.J., 1996, On Chip Morphology, Tool Wear, and Cutting Mechanics in Finish Hard Turning, Annals of the CIRP, 45/1:77-82.
- [6] Shaw, M.C., Vyas, A., 1993, Chip Formation in the Machining of Hardened Steel, Annals of the CIRP, 42/1:29-33.
- [7] Deshayes, L., Mabrouki, T., Ivester, R., Rigal, J-F., 2004, Serrated Chip Morphology and Comparison with Finite Element Simulations, Proceedings of 2004 ASME International Mechanical Engineering Congress and Exhibition, 1/1:1-10.
- [8] Komanduri, R., Turkovich, B.F., 1981, New Observations on the Mechanism of Chip Formation when Machining Titanium Alloys, Wear, 69/1:179-188.
- [9] Deshayes, L., Ivester, R., Batzer, S.A., Evans, J.L., Bhat, D.G., Whitenton, E.P., 2005, Mechanical and Thermal Behavior for Machining Ti-6Al-4V with AlMgB and WC-CO Tools. ASME International Mechanical Engineering Congress and Exhibition, MED, 16/1:503-511.
- [10] Campbell, C., Bendersky, L., Boettinger, W., Ivester, R., 2006, Microstructural characterization of Al-7075-T651 chips and work pieces produced by high-speed machining, Materials Science and Engineering A, 430/1:15-26.
- [11] Barry, J., Byrne, G., 2002, The Mechanisms of Chip Formation in Machining Hardened Steels, Journal of Manufacturing Science and Engineering, Transactions of the ASME, 124/1:528-535.
- [12] Barry, J., Byrne, G., 2002, Chip Formation, Acoustic Emission and Surface White Layers in Hard Machining, Annals of the CIRP, 51/1:65-70.
- [13] Davies, M.A., Burns, T.J., Evans, C.J., 1997, On the Dynamics of Chip Formation in the Machining of Hardened Steel, Annals of the CIRP, 46/1:25-30.
- [14] Bell, A., Ramalingam, S., Black, J., 1973, Metal Cutting Studies As Performed In The SEM, Transactions of the North American Manufacturing Research Institute, 2/1:99-110.
- [15] Vyas, A., Shaw, M.C., 1999, Mechanics of Saw-Tooth Chip Formation in Metal Cutting, Journal of Manufacturing Science and Engineering, 121/2:163-172.
- [16] Elbestawi, M.A., Srivastava, A.K., and El-Wardany, T.I., 1996, A Model for Chip Formation During the Machining of Hardened Steel, Annals of the CIRP, 45/1:71-76.
- [17] Poulachon, G., and Moisan, A., 1998, A Contribution to the Study of the cutting Mechanisms During High Speed Machining of Hardened Steel, Annals of the CIRP, 47/1:73-76.
- [18] Marusich, T.D. and Ortiz, M., 1995, Modeling and simulation of high speed machining, International Journal of Numerical Methods in Engineering, 38/21:3675-3694.
- [19] Taylor, B.N., and Kuyatt, C.C., 1994, Guidelines for Evaluating and Expressing the Uncertainty of NIST Measurement Results, NIST Technical Note 1297.

Surface Speed (m/min)	Cutting Force (N)				Thrust Force (N)			
	Experimental		Simulation		Experimental		Simulation	
	Mean	2 σ	Mean	2 σ	Mean	2 σ	Mean	2 σ
0.3 mm/rev feed rate								
200	1585	209	1961	239	806	239	667	169
250	1538	226	1912	243	759	162	641	112
300	1541	247	1888	309	735	199	630	194
400	1535	269	1849	330	697	176	606	207
500	-	-	1822	349	-	-	591	213
600	1599	330	-	-	660	152	-	-
0.15 mm/rev feed rate								
200	959	108	1144	144	600	38	436	143
300	-	-	1135	63	-	-	430	27
400	908	98	1102	169	511	30	415	142
500	888	53	1042	87	495	16	378	52

Table 1: Cutting and thrust force analysis results

Surface Speed (m/min)	SEGMENTATION PERIOD (μ s)									
	Experimental						Simulation			
	Min	Max	Mean	Median	Mode	2 σ	Mean	Median	Mode	2 σ
0.3 mm/rev feed rate										
200	117	533	238	217	183	149	113	111	N/A	30
250	67	300	172	175	183	102	93	91	N/A	15
300	50	500	139	133	100	127	79	80	N/A	12
400	33	217	98	100	100	70	60	60	N/A	9
500	-	-	-	-	-	-	47	48	N/A	9
600	17	117	66	67	67	38	-	-	-	-
0.15 mm/rev feed rate										
200	67	500	169	167	200	123	No segmentation			
300	-	-	-	-	-	-	36	35	N/A	6
400	33	167	76	67	67	51	30	30	N/A	8
500	17	150	58	50	50	48	23	23	N/A	6

Table 2: Segmentation period analysis results

Surface Speed (m/min)	WORKPIECE LENGTH PER SEGMENT (mm)									
	Experimental						Simulation			
	Min	Max	Mean	Median	Mode	2 σ	Mean	Median	Mode	2 σ
0.3 mm/rev feed rate										
200	0.389	1.778	0.792	0.722	0.611	0.495	0.370	0.381	N/A	0.090
250	0.278	1.250	0.715	0.729	0.764	0.426	0.389	0.398	N/A	0.047
300	0.250	2.500	0.697	0.667	0.500	0.633	0.393	0.384	N/A	0.078
400	0.222	1.444	0.654	0.667	0.667	0.468	0.399	0.398	N/A	0.069
500	-	-	-	-	-	-	0.397	0.398	N/A	0.061
600	0.167	1.167	0.658	0.667	0.667	0.378	-	-	-	-
0.15 mm/rev feed rate										
200	0.222	1.667	0.564	0.556	0.667	0.409	No segmentation			
300	-	-	-	-	-	-	0.177	0.180	N/A	0.024
400	0.222	1.111	0.510	0.444	0.444	0.340	0.196	0.195	N/A	0.039
500	0.139	1.250	0.487	0.417	0.417	0.397	0.195	0.194	N/A	0.047

Table 3: Workpiece length per segment analysis results